Process modeling of contact extrusion and coextrusion

Robert B. Secor

Senior process engineer, 3M Engineering Systems and Technology, 3M Center Bldg. 518-1-01, St. Paul, MN 55144-1000

ABSTRACT *Successful contact extrusion of single-layer or multiple-layer films is achieved by controlling the materials and processes. Die geometry, operational modes, and the rheological properties of the extruded liquids influence the extrusion mechanics. Process models based on physical mass and momentum balances have been constructed to elucidate these relationships between materials and processes. The models portray how the rheological properties of the liquid influence the operation of contact extrusion and coextrusion. Shear-sensitive viscosity and elastic normal stresses are the important rheological properties that have been incorporated into the process models.*

KEYWORDS
Extrusion coating
Mathematical analysis
Nonwovens
Rheology
Shear stress
Viscosity

Contact extrusion refers to the coating or extrusion operations in which the liquid stream emanating from a die is confined in the narrow knifing channel formed by the die and the substrate and/or backup roller (**Fig. 1**). The gap in the channel is necessarily less than twice the thickness of the final coated layer.

Presented here are process models that relate the geometric and operational aspects of contact extrusion to the rheological properties of the liquid. The interplay between these ramifications defines a number of process responses that delineate operational conditions for the contact extrusion process. Although deformable backup rollers are sometimes employed, the analysis presented here is restricted to rigid backup rollers.

Mathematical model—knifing channel

The basic principles that govern the flow of liquid through a knifing channel and the subsequent formation of a liquid layer on the moving surface are the balance of force and momentum and the conservation of mass. These two principles constitute the familiar equations of motion.

Regarding only steady, two-dimensional flow and low rates of convergence and divergence everywhere within the wetted channel, let us consider that the flow will have a predominant direction. This generalization will allow us to neglect both the variation in cross-stream pressure and the streamwise diffusion of momentum, reducing the equations of motion to:

$$\rho u \frac{\partial u}{\partial x} + \rho v \frac{\partial u}{\partial y} = -\frac{dp}{dx} + \frac{\partial \tau_{yx}}{\partial y} + \frac{\partial \tau_{xx}}{\partial x} + \rho g f_x \quad (1)$$

$$\frac{\partial u}{\partial x} + \frac{\partial v}{\partial y} = 0 \quad (2)$$

In these equations, u and v are the directional components of velocity in the spatial coordinates x and y, respectively, for which orientations are shown in Fig. 1. The variable p is the pressure referenced to the surrounding atmosphere (i.e., gauge pressure).

The relationship between the shear stress, τ_{yx}, and the rate of shear deformation, $\partial u/\partial y$, is governed by the liquid viscosity, as given in Eq. 3.

$$\tau_{yx} = \eta(\dot{\gamma}) \frac{\partial u}{\partial y} \quad \text{and} \quad \dot{\gamma} = \left| \frac{\partial u}{\partial y} \right| \quad (3)$$

In addition to shear stress, the flow of elastic liquids through the knifing channel may also give rise to normal stresses. If liquid elasticity is fully developed—that is, if the liquid's "memory" time is short in comparison to its residence time in the knifing channel—the elastic normal stresses are related to the rate of shear deformation by the first and second normal stress coefficients.

$$\tau_{xx} = [\Psi_1(\dot{\gamma}) + \Psi_2(\dot{\gamma})]\,\dot{\gamma}^2 \quad \text{and}$$
$$\tau_{yy} = [\Psi_2(\dot{\gamma})]\,\dot{\gamma}^2 \quad (4)$$

Much less is known about the behavior of the normal stress coefficients than is known about the liquid viscosity. The normal stress coefficients are probably independent of shear rate at very low rates and often decrease faster than the viscosity does with increasing deformation rates. Often the second normal stress coefficient is an order of magnitude smaller than the first normal stress coefficient and has the opposite sign.

The boundary conditions of no-slip and impenetrability applied at the

1. Diagram of contact extrusion

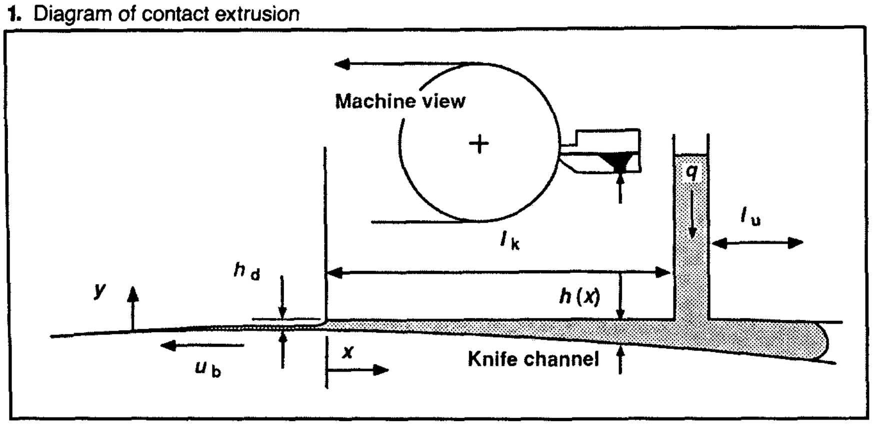

moving surface and the knife surface are represented by Eqs. 5 and 6.

At $y = 0$,

$$u = -u_b \text{ and } v = 0 \qquad (5)$$

At $y = h(x)$, $0 \leq x \leq l_k$,

$$u = 0 \text{ and } v = 0 \qquad (6)$$

where u_b is the speed of the backup roller and $h(x)$ is the coating gap in the knifing channel of length l_k.

It is necessary to specify the knifing channel geometry to solve the balance equations of mass and momentum. If the backup roller is rigid, the knife channel geometry is decoupled from liquid flow through the channel. In this case, the channel geometry can be described mathematically to a close approximation by a quadratic equation.

$$h(x) = h_d + (\tan\alpha)x + \frac{1}{R_b}\frac{x^2}{2} + O\left(\frac{x^4}{8R_b^3}\right) \qquad (7)$$

In Eq. 7, R_b is the radius of the backup roller, and α is the angle of rotation about the downstream knife edge. The specification of the lateral offset between the knife and backup roll centers, Δl, is an equivalent description to the knife rotation angle:

$$\tan\alpha = \Delta l / R_b \qquad (8)$$

Appropriate scaling of this problem leads to the dimensionless variables in Eq. 9.

$$X = \frac{x}{l_k}, \quad Y = \frac{y}{h_d}, \quad H = \frac{h}{h_d},$$

$$U = \frac{u}{u_b}, \quad V = \frac{v l_k}{u_b h_d}, \quad P = \frac{p h_d^2}{l_k \eta^* u_b},$$

$$T_{yx} = \frac{h_d\,\tau_{yx}}{\eta^* u_d}, \; T_{xx} = \frac{h_d^2\,\tau_{xx}}{\Psi_1^* u_b^2}, \; T_{yy} = \frac{h_d^2\,\tau_{yy}}{\Psi_2^* u_b^2} \qquad (9)$$

In this equation, the characteristic viscosity and normal stress coefficients are evaluated at the characteristic shear rate.

$$\eta^* = \eta(\dot\gamma^*),\; \Psi_1^* = \Psi_1(\eta^*),\; \Psi_2^* = \Psi_2(\dot\gamma^*),$$
$$\dot\gamma^* = \frac{u_b}{h_d} \qquad (10)$$

The equation set in dimensionless form is as presented in Eqs. 11–15.

$$Re\,\frac{h_d^2}{l_k^2}\left[U\frac{\partial U}{\partial X} + V\frac{\partial U}{\partial Y}\right] =$$
$$-\frac{dP}{dX} + \frac{\partial T_{yx}}{\partial Y} + (SR_1 + SR_2)\,\frac{l_k}{h_d}\frac{\partial T_{xx}}{\partial X}$$
$$+ St\,f_x \qquad (11)$$

$$\frac{\partial U}{\partial X} + \frac{\partial V}{\partial Y} = 0 \qquad (12)$$

$$U = -1,\; V = 0 \text{ at } Y = 0 \qquad (13)$$

$$U = 0,\; V = 0 \text{ at } Y = H(X),\; 0 \leq X \leq 1 \qquad (14)$$

$$H(X) = 1 + G_{incl}\,X + G_{curv}\,\frac{X^2}{2} \qquad (15)$$

In these equations, the Reynolds number, Stokes number, and stress ratio are defined in Eq. 16.

$$Re \equiv \frac{\rho\,u_b l_k}{\eta^*},\quad St \equiv \frac{\rho\,g\,h_d^2}{\eta^*\,u_b},$$
$$SR_1 \equiv \frac{\Psi_1^*\,\dot\gamma^*}{\eta^*},\quad SR_2 \equiv \frac{\Psi_2^*\,\dot\gamma^*}{\eta^*} \qquad (16)$$

The dimensionless geometric parameters, referred to as "inclination" and "curvature" are defined in Eq. 17 as G_{incl} and G_{curv}, respectively.

$$G_{incl} \equiv \frac{l_k}{h_d}\tan\alpha = \frac{l_k}{h_d}\frac{\Delta l}{R_b}$$
$$G_{curv} \equiv \frac{l_k^2}{h_d R_b} \qquad (17)$$

Under ordinary operating conditions, the effect of viscous shear far outweighs that of inertia and gravity in controlling the flow. Such conditions prevail when

$$Re\,(h_d^2/l_k^2) << 1$$
$$St << 1 \qquad (18)$$

correspondingly. Under these conditions, the equation set is reduced further by eliminating the inertial and gravitational terms.

$$\frac{dP}{dX} = \frac{\partial T_{yx}}{\partial Y} + (SR_1 + SR_2)\,\frac{l_k}{h_d}\frac{\partial T_{xx}}{\partial X} \qquad (19)$$

Except for the normal stress term, this is the familiar lubrication approximation.[1]

Mathematical model—edges of the knifing channel

The flow of liquid in the immediate vicinity of the downstream edge of the knife is inherently two-dimensional. To gauge the effects of this flow regime on the operating behavior of contact extrusion, a macroscopic force balance is performed on the region, as shown in **Fig. 2.**

The control volume shown starts a distance δ inside the knifing channel, where the flow approximations used in the knifing channel start to fail. This control volume for the force balance extends far downstream to a point where viscous stresses that developed in the knifing channel have dissipated.

The forces in the main flow direction that act on the control volume are pressure, normal stress, and inertia on the in-flow boundary, inertia and ambient pressure on the out-flow boundary, and shear stress and interfacial tension on the control volume sides. The balance of these forces results in the expression of Eq. 20.

See Eq. 20.

By dropping the inertial, gravitational, and surface tension terms and converting to dimensionless form, the force balance becomes as expressed in Eq. 21.

See Eq. 21.

Here the superscript "LA" refers to the stresses corresponding to the lubrication approximation solution. The terms on the right side of Eq. 21 represent the effects of the flow

[1]Cameron, A., Basic Lubrication Theory, 3rd edn., Ellis Horwood Ltd., Chichester, England, 1981.

rearrangement and the relaxing shear stress at the liquid-substrate interface. According to Tanner *et al.*,[2] these terms can be neglected with minimal error.

Under these assumptions, the pressure at the downstream edge of the knife is equal to the normal stress developed in the knife channel.

$$P(0) = SR_1 \frac{l_k}{h_d} \int_0^1 (T_{xx})_{X=0}\, dY \qquad (22)$$

Similar tactics are required around the feed slot and at the upstream liquid heel. To relate the liquid pressures on either side of the feed slot, a macroscopic force balance is again performed, this time around the feed slot. With the same assumptions, the force balance becomes as expressed in Eq. 23:

$$P(1^+)\, H(1^+) - SR_1 \frac{l_k}{h_d} \int_0^{H(1^+)} [T_{xx}]_{X=1^+}\, dY =$$

$$P(1^-)\, H(1^-) - SR_1 \frac{l_k}{h_d} \int_0^{H(1^-)} [T_{xx}]_{X=1^-}\, dY \qquad (23)$$

where the + and - superscripts denote the conditions just upstream and just downstream of the inlet.

In contact extrusion, it is essential to control the flow of liquid in the channel upstream of the feed slot. Consequently, the modeling is extended into this region. With the exception of outlet and inlet conditions, the equation set is the same as that for the knifing channel. The conditions for the upstream flow are determined by another force balance: this time it is around the upstream heel in the knifing channel. Under the same assumptions made for the force balances, this balance becomes as expressed in Eq. 24.

$$P(1+L')\, H(1+L') = SR_1 \frac{l_k}{h_d} \int_0^{H(1+L')} T_{xx}\, dY \qquad (24)$$

In this equation, L' is the dimensionless length of the liquid in the channel upstream of the feed slot.

The combination of the lubrication approximation in the knifing channel and the force balances around the edges and feed slot of the contact extrusion die constitute a mathe-

2. Control volume for the force balance at the downstream edge of the contact extrusion die

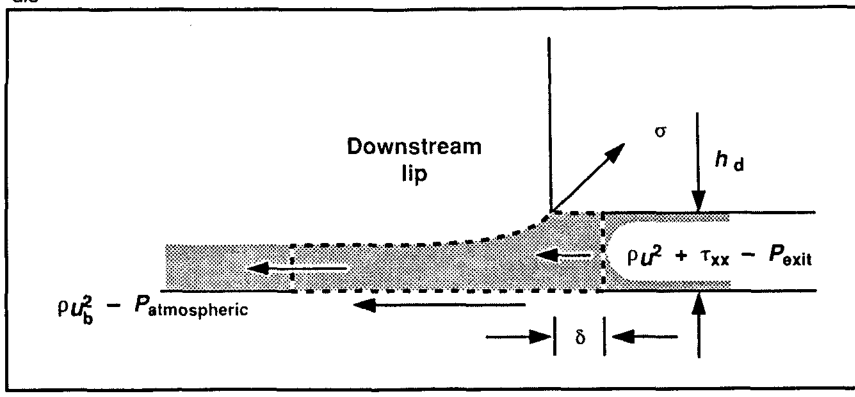

matical model for the contact extrusion flow. In general terms, the problem statement of the theoretical model of the flow is reduced to a function of two geometric parameters and a set of rheological ones, as presented in Eq. 25.

$$U(X,Y),\ V(X,Y),\ P(X) = \text{Function}\left\{ \begin{matrix} G_{incl},\ G_{urv},\ (SR_1 + SR_2)\ \frac{h_d}{l_k}, \\ \frac{\eta(\dot\gamma)}{\eta^*},\ \frac{\Psi_1(\dot\gamma)}{\Psi_1^*},\ \frac{\Psi_2(\dot\gamma)}{\Psi_2^*} \end{matrix} \right\} \qquad (25)$$

Numerical implementation

To transform Eq. 19 into a form suitable for implementation in a numerical algorithm, the equation is first integrated across the thickness dimension of the knifing channel.

$$\frac{dP}{dX} = \frac{T_{xy}(X,H) - T_{yx}(X,0)}{H(X)} + (SR_1 + SR_2)\ \frac{l_k}{h_d}\ \frac{1}{H(X)} \int_0^{H(X)} \frac{\partial T_{xx}}{\partial X}\, dY \qquad (26)$$

This operation is followed by integration across the length dimension.

See Eq. 27.

After switching the order of integration on the last term, Eq. 27 reduces to Eq. 28.

See Eq. 28.

Thus the pressure in the knifing channel is determined by both the viscous pressure drop represented by the first term in Eq. 28 and an elastic contribution at the ends represented by the last term.

Integrating the equation of continuity, Eq. 12, across the thickness of the knifing channel with the application of the boundary conditions of Eqs. 13 and 14 also leads to a reduced form.

$$\int_0^H \frac{\partial U}{\partial X} + \frac{\partial V}{\partial Y}\, dY = \frac{\partial}{\partial X} \int_0^H U\, dY = 0$$

$$\text{or} \qquad \int_0^H U\, dY = -T \qquad (29)$$

In Eq. 29, T is the dimensionless final coated film thickness.

$$T \equiv \frac{t}{h_d} \text{ and } t = -\frac{1}{u_b} \int_0^{h(x)} u\, dy \qquad (30)$$

Equations 28 and 29 form the basis of the numerical algorithm for the solution of the flow field in the knifing channel. Two methods are available for the execution of this task: (a) a conventional finite element solution of the velocity fields and (b) an alternative algorithm based on a novel approach that does not require the calculation of the velocity fields.

One-dimensional finite element formulation

In the conventional finite element solution of the equations of motion, the first step is to compute the viscous pressure drop in the knifing channel subject to the flow rate constraint.

$$\left(\frac{dp}{dx}\right)_{viscous} = \frac{\partial}{\partial y} \left[\eta(\dot\gamma)\ \frac{\partial u}{\partial y} \right] \qquad (31)$$

If the liquid layer consists of M different layers, flow rate constraints exist for each layer.

$$Q_i = -t_i u_b = -\int_{h_{i-1}}^{h_i} u\, dy \qquad (32)$$

where $i = 1,2,3,\ldots,M$

In Eq. 32, Q_i and t_i are the flow rate and final film thickness in Layer i.

[2]Tanner, R. I., Phan-Thien, N., and Dudek, J., Boundary conditions in viscoelastic lubrication, Proc. IX Intl. Congress on Rheology, Plenum Press, New York, 1984.

In the finite element formulation of this equation set for multilayered flows, we proceed by subdividing the one-dimensional domain between $y = 0$ and $y = h$ into N finite elements for each of the M liquid layers. Quadratic basis functions represent the unknown liquid velocity in each layer. The governing equations for these are the Galerkin-weighted residuals of the momentum balance equation (Eq. 33).

$$R_v^i = \int_0^h \phi^i \left[\frac{\partial}{\partial y} \left\{ \eta \frac{\partial u}{\partial y} \right\} - \left(\frac{dp}{dx} \right)_{vis} \right] dy = 0 \qquad (33)$$

Flow rate, position, and pressure gradient unknowns are introduced at each odd-numbered node. The governing equations for these are given collectively in Eqs. 34 and 35.

For the flow rate unknowns q_i,

$$q_1 = 0 \text{ and } q_i = q_{i-2} + \int_{h_{i-2}}^{h_i} u(y)\, dy$$

$$\text{where } i = 3,5,7,\ldots,2N+1 \qquad (34)$$

For the position unknowns h_i,

$$h_1 = 0 \text{ and}$$

$$h_{2N+1} = h \text{ and}$$

$$h_i = \frac{h_{i-2} + h_{i+2}}{2}$$

$$\text{where } i = 3,5,7,\ldots,2N-1 \qquad (35)$$

Equation 35 applies except when node i lies on the interface between liquid j and liquid j+1. Then the position equation is Eq. 36.

$$q_i = \sum_{k=1}^{k=j} Q_k \qquad (36)$$

The equation governing the viscous pressure gradient is given as Eq. 37.

$$p_{x,i} = p_{x,i+2}$$

$$\text{where } i = 1,3,5,\ldots,2N-1 \qquad (37)$$

except for at the last node, where the equation is

$$q_{2N+1} = \sum_{k=1}^{k=M} Q_k \qquad (38)$$

This total set composes a system well suited for solution by iterative techniques using sparse matrix solution techniques. A quasi-Newtonian iteration strategy using a frontal matrix solver is used to solve the set of algebraic equations of Eqs. 33-38.

Novel alternative algorithm

An alternative to the conventional finite element procedure outlined is the shear-sensitive lubrication algorithm. This algorithm locally relates the viscous pressure gradient to the flow rate per unit width using the flow rate constraint and a different form of the no-slip boundary conditions:

$$q = -\int_0^h u\, dy$$

$$-u_b = \int_0^h \frac{du}{dy}\, dy \qquad (39)$$

The application of integration by parts to the flow rate constraint followed by a variable transformation from the coordinate y to shear rate yields Eqs. 40 and 41.

$$q = \frac{-u_b\, \eta_0 \dot{\gamma}_0 h}{(\eta_1 \dot{\gamma}_1 - \eta_0 \dot{\gamma}_0)} - \frac{h^2}{(\eta_1 \dot{\gamma}_1 - \eta_0 \dot{\gamma}_0)^2}$$

$$\left[\left\{ \frac{1}{2}\, \eta^2 \dot{\gamma}^3 \right\}_{\dot{\gamma}_0}^{\dot{\gamma}_1} - \frac{1}{2} \int_{\dot{\gamma}_0}^{\dot{\gamma}_1} \eta^2 \dot{\gamma}^2 d\dot{\gamma} \right] \qquad (40)$$

$$\frac{-u_b(\eta_1 \dot{\gamma}_1 - \eta_0 \dot{\gamma}_0)}{h} =$$

$$\{\eta \dot{\gamma}^2\}_{\dot{\gamma}_0}^{\dot{\gamma}_1} - \int_{\dot{\gamma}_0}^{\dot{\gamma}_1} \eta \dot{\gamma}\, d\dot{\gamma} \qquad (41)$$

These two equations in conjunction with an expression for the streamwise pressure gradient, Eq. 42, completely specify the flow rate-pressure drop relationship, regardless of the viscosity behavior of the liquid.

$$h \frac{dp}{dx} = \eta_1 \dot{\gamma}_1 - \eta_0 \dot{\gamma}_0 \qquad (42)$$

In Eqs. 40-42, the subscript "1" denotes the substrate surface, and the subscript "0" denotes the die surface. Simultaneous solution of Eqs. 40 and 41 yields the shear rates at the upper and lower surfaces. The pressure gradient is then calculated from Eq. 42. The only requirements are that the viscosity function be known as a function of shear rate and that the integrals in Eqs. 40 and 41 can be evaluated either analytically or numerically.

Process response and the window of operability

The mathematical model for contact extrusion is useful for mapping out the process response to changes in the independent material, design, and operational parameters. From the computed velocity and pressure fields can be derived any of a number of dependent responses of the process over which some control is desired. Examples include the normal and shear forces acting on the die, as presented in Eq. 43, maximum shear rate, maximum pressure, and the presence of closed recirculations.

$$f_n = \int_0^{l_k + l_n} p - \tau_{yy}|_{y\,=\,h(x)}\, dx$$

$$f_s = \int_0^{l_k + l_n} \tau_{yx}|_{y\,=\,h(x)}\, dx \qquad (43)$$

The dimensionless forms of loading forces are as presented in Eq. 44.

See Eq. 44.

In addition to the process responses, some parameter choices will result in a failure mode of operation. Four types of failure are observed in contact extrusion:

1. Liquid dewetting
2. Starvation
3. Leaking
4. Die–roller contact.

Liquid dewetting occurs at the downstream lip of the knife channel when the stress inside the channel is lower than the surrounding atmospheric pressure. The lower stress causes a tendency for liquid to detach from the die lip and causes streaks in the final film. Starvation occurs when the liquid flow rate is insufficient to fill the knife channel downstream of the feed slot. Leaking occurs when the liquid heel upstream of the feed slot is not contained by the die. Loss of liquid metering and oscillatory behavior are common results. Finally, die–roller contact occurs when there is a geometric conflict between the operating mode of the die and the location of the backup roller.

Figure 3 shows these failure modes in an operating diagram for contact extrusion of a single layer of a Newtonian liquid. **Figures 4 and 5** show the corresponding diagrams for shear-thinning and elastic materials. Within the operating diagrams, contours of the length of the coating bead in the upstream knife channel are plotted. Note the opposing effects of shear sensitivity and elasticity on the shape of the operating diagram.

When two layers of liquid are coated in contact extrusion, several operating states are possible. When the coating gap is less than about three times the thickness of the bottom layer, the

3. Operability diagram for a Newtonian liquid (curvature = 1)

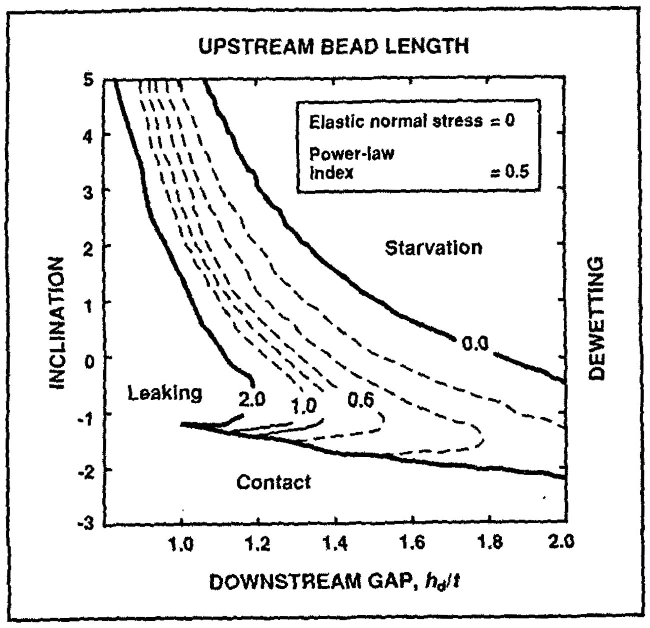

4. Operability diagram for a shear-thinning liquid with a power-law index equal to 0.5 (curvature = 1)

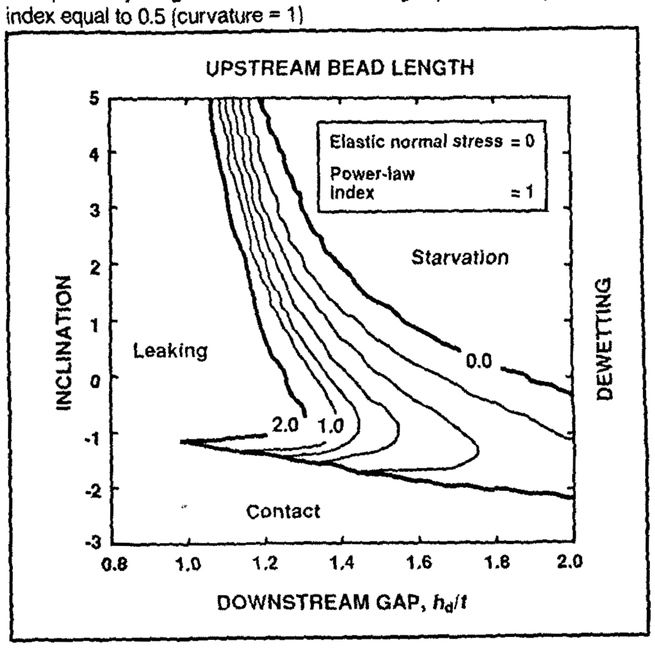

5. Operability diagram for a liquid that is shear-thinning but also elastic (curvature = 1)

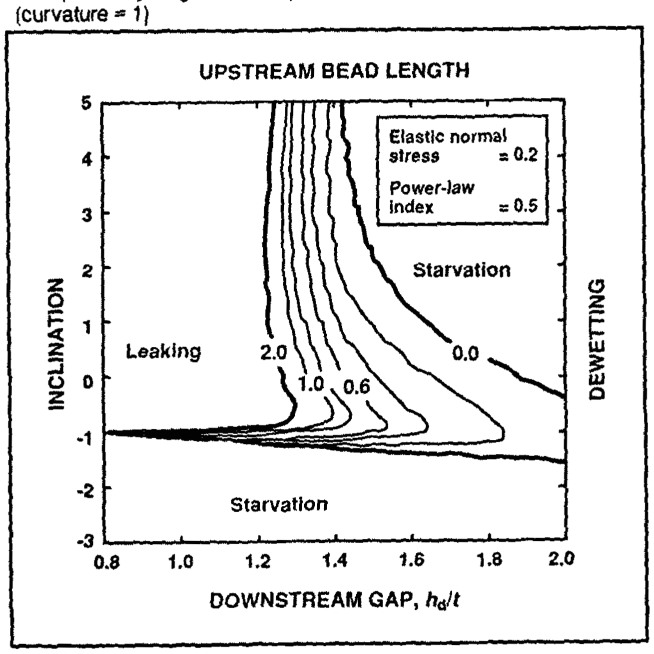

6. Operability diagram for dual-layer extrusion when the two layers have equal thicknesses (curvature = 1)

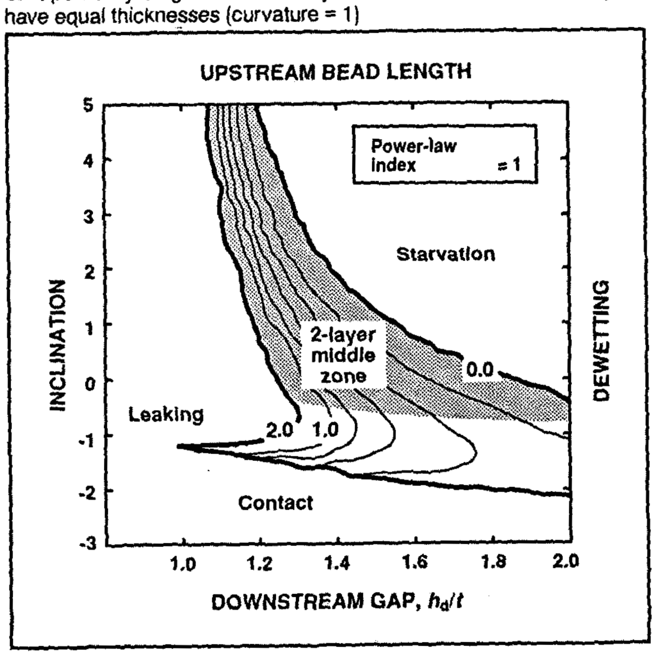

upper layer occupies only the downstream section of the knife channel.

At larger gaps, the upper layer can invade upstream toward the bottom layer feed slot. This produces both a slowly moving zone of liquid that is susceptible to thermal degradation and an operating state that is extremely sensitive to external disturbances. Both make this operating state undesirable.

At still larger gaps, a third operating state is possible, in which a three-layer structure is formed in the channel upstream of both feed slots.

The different operating states possible in two-layer contact coextrusion pose additional bounds on the operating diagrams, as illustrated in **Fig. 6**. The figure shows the condition for a two-layer stagnant zone between the two feed slots superimposed on the operating diagram for a Newtonian liquid. The extent of the operating diagram is substantially reduced in this case.

Summary

Process models have been constructed that show the relationships between geometric, rheological, and operational parameters in contact extrusion and coextrusion. These models take into account the differences in the behavior of shear-thinning and elastic liquids. Compared to single-layer extrusion, the operating diagrams for contact extrusion of multiple layers are more complex.☐

Received for review June 5, 1991.
Accepted July 31, 1991.

Presented at the TAPPI 1991 Polymers, Laminations and Coatings Conference.

Nomenclature

Variables

f = directional vector of the gravitational force
g = acceleration of gravity, m/s²
h = coating gap, m
l = length, m
Δl = lateral offset, m
p = gauge pressure, Pa
t = film thickness, m
u = directional component of velocity in the x direction, m/s
v = directional component of velocity in the y direction, m/s
x, y = spatial coordinates, with orientations defined in Fig. 1, m
G_{incl} = geometric parameter of inclination
G_{curv} = geometric parameter of curvature
$O(x)$ = on the order of magnitude of x
Q = flow rate, m³/s
R = radius, m
Re = Reynolds number
St = Stokes number
SR = stress ratio

Greek characters

α = knife rotation angle
δ = distance inside the knifing channel
$\dot{\gamma}$ = shear rate, s⁻¹
η = viscosity, Pa•s
ρ = liquid density, kg/m³
σ = surface tension, Pa/m
τ = shear stress, Pa
Ψ = normal stress coefficient, Pa•s²

Index subscripts

b = backup roller
k = knifing channel
$+$ = just upstream of the inlet
$-$ = just downstream of the inlet

For Figs. 3-6

$(l_k/t)\tan\alpha$ = inclination
$(\Psi_1 u_b)/(\mu^* l_k)$ = elastic normal stress
$l_k^2/(t\,R_b)$ = curvature
n = power-law index

Equations

$$\int_0^{h_d} (p - \tau_{xx})\,dy = \rho\,u_b^2\,t - \int_0^{h_d} \rho\,u^2\,dy + \rho\,g\,f_x \left[h_d\,\delta + \int_{-\infty}^{0} h'\,dx \right] + \int_0^{\delta} \tau_{yx}|_{y=h_d}\,dx - \int_{-\infty}^{\delta} \tau_{yx}|_{y=0}\,dx - \int_{-\infty}^{0} \frac{\sigma \dfrac{dh'}{dx} \dfrac{d^2 h'}{dx^2}}{\left[1 + \left(\dfrac{dh'}{dx}\right)^2\right]^{3/2}}\,dx \tag{20}$$

$$P(0) - SR_1 \frac{l_k}{h_d} \int_0^1 (T_{xx})_{X=0}\,dY = -\int_{-\infty}^{0} T_{yx}|_{Y=0}\,dX + \int_0^{\Delta} [T_{yx} - T_{yx}^{LA}]_{Y=1} - [T_{yx} - T_{yx}^{LA}]_{Y=0}\,dX \tag{21}$$

$$P(X) - P(0) = \int_0^X \frac{T_{yx}(H) - T_{yx}(0)}{H(X')}\,dX' + (SR_1 + SR_2)\frac{l_k}{h_d} \int_0^X \frac{1}{H(X')} \int_0^{H(X')} \frac{\partial T_{xx}}{\partial X}\,dY\,dX' \tag{27}$$

(Continued on next page)

$$P(X) - P(0) = \int_0^X \frac{T_{yx}(H) - T_{yx}(0)}{H(X')} \, dX' + (SR_1 + SR_2) \frac{l_k}{h_d} \left[\frac{1}{H(X)} \int_0^{H(X)} T_{xx} dY - \frac{1}{H(0)} \int_0^{H(0)} T_{xx} \, dY \right] \tag{28}$$

$$F_n \equiv \frac{f_n h_d^2}{l_k^2 u_b \eta^*} = \int_0^{1+L'} P - SR_2 \frac{h_d}{l_k} T_{yy}\big|_{Y=H(X)} \, dX$$

$$F_s \equiv \frac{f_s h_d}{l_k u_b \eta^*} = \int_0^{1+L'} T_{yx}\big|_{Y=H(X)} \, dX \tag{44}$$